

# Transient Rotor Drop Evaluation of AMB Machinery

R. G.. Kirk

*Mechanical Engineering Department  
Virginia Polytechnic Institute and State University  
Blacksburg, Virginia, USA*

E. J. Gunter

RODYN Vibration Analysis, Inc.  
Charlottesville, VA USA

W. J. Chen

Ingersoll-Rand Company  
800-B Beatty Street  
Davidson, NC 28036

## ABSTRACT

A major limitation of AMB supported machinery is their dependence on auxiliary or backup bearings in the event that the magnetic bearings lose power due to control system failure. These backup bearings should be designed to withstand the severe loads encountered after the AMB failure when the rotor drops onto them. This has prompted the development of general purpose finite element based, non-linear transient analysis programs capable of evaluating shock loading, blade loss and rotor drop phenomena experienced in rotors supported by AMBs. Previous testing and results have been made for a single AMB drop or both AMBs of a two bearing rotor. The current interest also includes the multiple AMB supported machinery systems, i.e., systems with more than two AMB or auxiliary bearings. This paper reviews the method of rotor drop analysis for AMB bearing systems. A commercially available program, DyRoBeS, is then applied to four different rotor designs to evaluate their rotor drop transient response. The total power loss rotor drop results of the ISO NEDO test rotor will be discussed for assumed backup bearing conditions. Three other AMB support machines will be briefly discussed.

## INTRODUCTION

The rotor dynamic evaluation of turbomachinery plays an important role in the overall design process of all new rotating machines. The proper design of any AMB system requires the knowledge of all the dynamic loads that will ever be experienced by the rotor in its planned service. One of the major setbacks of the current high performance turbomachinery equipped with a AMB systems is their dependence on auxiliary or back-up bearings to support the rotor in case the AMB control system fails. These backup bearings have failed to withstand various dynamic loads in the event of AMB failure during both controlled test stand and field operating conditions. This motivated researchers to analytically predict the motion of the rotor and the impact loads subjected to the backup bearing following AMB failure. Ishii (1990) applied transient response technique to simulate the rotor drop phenomena and predict the high instantaneous loads acting on the backup bearing. He performed the transient response analysis to simulate the rotor drop phenomenon for a two mass Jeffcott rotor system using the Runge-Kutta fourth order method. Gelin, Pugno and Hagopian (1990) studied the dynamic behavior of rotors on safety auxiliary bearings. Ishii and Kirk (1991) described some analytical results on rotor drop and instantaneous loads on flexible backup bearings for a Jeffcott rotor model. Fumagalli, Feeny and Schweitzer (1992) and Fumagalli, Varadi and Schweitzer (1994) studied the dynamics and loads of a rigid rotor in a rigid bearing with clearance. Kirk and Ishii (1993) extended their analytical capability by making improvements to their earlier model to more accurately simulate the actual flexible

support systems. The vibrational behavior of a one ton compressor rotor being dropped into the auxiliary bearings after AMB failure has been reported by Schmied and Pradetto (1992).

The need for a better understanding of the dynamics of the rotor drop phenomena, lead Kirk, et. al. (1994) to set up a full scale test rig to evaluate various backup bearing configurations and to develop analytical tools to simulate complex turbomachinery supported by AMBs. Ramesh and Kirk (1992) developed computational ability to perform finite element based steady state analysis of AMB turbomachinery and compared their results with experimental data. Raju, Ramesh, Swanson and Kirk (1995) presented analytical results for finite element based rotor drop simulation and successfully compared them with experimental data. These simulations were done for cases with rigid backup bearings. The capability of the analytical tool was later enhanced by Raju (1996), to take into account, various types of support flexibilities. Swanson, Raju and Kirk (1996) and Kirk, Raju and Ramesh (1996) presented some of the results obtained using that computer program. The current industrial design interests are for the drop of AMB supported rotor systems, including the controller degrees of freedom and also including two or more non linear backup bearings. Modern design analysis also requires a more advanced pre and post processor for initial model generation and presentation of the results. The results presented in this paper to evaluate the stability of multiple bearing rotor drop, were generated using a commercial computer program, DyRoBeS (Chen, 1998 ).

### Finite Element Modeling Of General Rotor-Bearing Systems

The process of theoretically modeling any physical system for numerical simulation purposes consists of isolating the parameters influencing the dynamic nature of that system and developing the mathematical equations which represent the actual system as closely as possible. These equations are then solved using optimum numerical methods to obtain the desired results for predicting the actual system dynamics. The current process of modeling turbomachinery supported by AMBs requires the knowledge of finite element discretization of rotor-bearing systems. In addition, the various numerical methods capable of efficiently performing transient analysis using the dynamic equilibrium equations of this particular system must be considered to provide the best solution technique. The influence and relationships of various parameters are described in more detail in the following discussion. The dynamic equilibrium equation for a rotor-bearing system can be represented in matrix form as follows when the speed of operation is constant:

$$M\ddot{q} + C\dot{q} + Kq = F \quad (1)$$

where  $M$ ,  $C$ , and  $K$  are the mass, damping and stiffness matrices obtained from finite element discretization. The state vectors  $\ddot{q}$ ,  $\dot{q}$  and  $q$  are the acceleration, velocity and displacement vectors of the system.  $F$  is the external force vector which propels the system. The shaft also known as rotor element is modeled as a beam element. The disks and turbine blades are modeled as discrete external mass elements having inertia and mass properties. Bearings, seals, etc. are modeled as discrete elements having stiffness and damping. The Z-axis of the reference frame coincides with the centerline of the rotor element. The displacement vector for the global finite element matrices can be written as :

$$q = \{x_1, y_1, \theta_{x1}, \theta_{y1}, x_2, y_2, \theta_{x2}, \theta_{y2}, \dots, x_n, y_n, \theta_{xn}, \theta_{yn}\}^T \quad (2)$$

where 'n' is the number of nodes in the global finite element model.

The acceleration vector  $\ddot{q}$  and velocity vector  $\dot{q}$  are in the same order as the displacement vector. The external force vector  $F$  is also in the same order. Forces are applied along the

translational degrees of freedom at each node and moments are applied about the axis in which the corresponding degree of freedom rotates.

### **Forces on Rotors Supported by Active Magnetic Bearings**

Simulation of rotating machinery requires the knowledge of all the static and dynamic forces or loads acting on the system. Loads due to gravity, bearing misalignment, gear forces or steady maneuvers, do not change with time and are known as static loads. Loads that change with time such as imbalance, blade loss, and loading from aerodynamic effects or compressor surge are known as dynamic loads. Non-linear transient analysis can be performed with the finite element model of rotor-bearing systems using a direct integration method by taking into effect the influence of some of the above mentioned static and dynamic loads. In the case of rotating machinery supported on magnetic bearings, the number of effective components of the external force vector differ depending upon whether the bearings are active or not. The axial movement of the nodes in the rotor model and the presence of the thrust magnetic bearing are ignored in this discussion. In the following sections, the various forces taken into consideration for the analysis have been described in more detail. This description of forces has been separated into two sections: those which exist when the magnetic bearing has power and those which exist during and after the initial drop.

### **Forces Before AMB Power Loss**

The forces that were considered in the analysis when the rotor was supported on active magnetic bearings during normal operation were the imbalance force, gravity force, preloads applied at the AMB locations and the force due to AMB stiffness and damping. The equations used to model each of these forces are given in the following sub-sections.

#### **Imbalance:**

The imbalance forces in rotating machinery are generally seen in the planes having rigid disks, turbine blades, impellers, or couplings. The components of this force in the direction of the fixed reference X and Y axes of the finite element system can be obtained by the following equations for the case of constant speed of operation:

$$F_{u,x} = m\omega^2 \cos(\omega t + \alpha) \quad (3)$$

$$F_{u,y} = m\omega^2 \sin(\omega t + \alpha) \quad (4)$$

The term ' $\omega t + \alpha$ ' gives the angular position of the unbalance mass ' $m$ ' at time ' $t$ ' in the cross-section of the unbalance plane when the rotor is rotating at the speed ' $\omega$ '. The global force vector due to unbalance is:

$$\mathbf{F} = \{F_{u,x1}, F_{u,y1}, 0, 0, F_{u,x2}, F_{u,y2}, 0, 0, \dots, F_{u,xn}, F_{u,yn}, 0, 0\}^T \quad (5)$$

### **Magnetic Bearing Force**

The magnetic bearing stiffness and damping are non-linear functions of the rotor whirl frequency. In general, during analysis, constant or linearized AMB stiffness and damping properties at a particular running speed of interest are considered as illustrated in Fig. 1. These values had previously been supplied by the manufacturer or calculated by modeling the control system dynamics. The forces due to linearized bearings and seals can be assumed to have the following form:

$$\mathbf{F}_{amb} = \mathbf{C}_{amb} \dot{\mathbf{q}}_{amb} + \mathbf{K}_{amb} \mathbf{q}_{amb} \quad (6)$$

where,  $\mathbf{q}_{amb} = \{x_{amb}, y_{amb}\}^T$

$$\mathbf{K}_{amb} = \begin{bmatrix} k_{xx} & k_{xy} \\ k_{yx} & k_{yy} \end{bmatrix} \quad \text{and} \quad \mathbf{C}_{amb} = \begin{bmatrix} c_{xx} & c_{xy} \\ c_{yx} & c_{yy} \end{bmatrix}$$

In the case of magnetic bearing stiffness and damping, the cross-coupled terms are zeros.

Two additional options are used to model the active magnetic bearing in DyRoBeS. The linear Proportional-Integral-Derivative controller with low pass filter is used in the steady state analysis (Stability and Forced Response Analyses). The nonlinear active magnetic bearing requires more input data and is used in the non-linear transient analysis. For both options, the sensor stations may be different than the bearing stations (sensor non-collocation) and the model may be different for the two bearing axes.

### Active magnetic Bearing 1 – Linear PID controller with low pass filter

This bearing is modeled as a PID controller in series with a unity gain, first order low pass filter (generally used to model the amplifier). Two additional degrees of freedom will be added to each of the x and y equations to model the controller states for each bearing. However, these two additional degrees of freedom will not be available for displaying in the post-processor. The output of the PID controller at each axis is:

$$C_p x_s + C_i \int x_s dt + C_d \dot{x}_s \quad (7)$$

Where  $x_s$  is the displacement at sensor location. The control force at each direction in the S-domain is:

$$F = \left( C_p + C_i \frac{1}{S} + C_d S \right) \left( \frac{2\pi f_c}{S + 2\pi f_c} \right) x_s \quad (8)$$

### Active Magnetic Bearing 2 – Non-Linear Transient Analysis

This bearing is a standard PID controlled active magnetic bearing with sensor non-collocation, gap non-linearity and current saturation effects for the transient analysis only. The control current is determined from the following expression:

$$i_c = C_p x_s + C_i \int x_s dt + C_d \dot{x}_s \quad (9)$$

The currents supplied to the magnetic bearing are determined from the following:

$$i_1 = i_{b,p} - i_c$$

$$i_2 = i_{b,n} + i_c$$

$$\text{if } i < 0, \quad i = 0; \quad \text{if } i > i_{\text{limit}}, \quad i = i_{\text{limit}}$$

The force in the magnetic bearings is:

$$F = F_C \cdot \left[ \left( \frac{i_1}{h_1} \right)^2 - \left( \frac{i_2}{h_2} \right)^2 \right] \quad (10)$$

where

$$h_1 = \text{gap} - x_b$$

$$h_2 = \text{gap} + x_b$$

### **Gravity Load:**

The load on the rotor ' $F_g$ ' due to the acceleration due to gravity 'g' is a constant or static load distributed over the mass of the rotor. It can be calculated by multiplying the global mass matrix  $M$  with the acceleration vector ' $a_g$ '.

$$F_g = M a_g \quad (11)$$

$$\text{where, } a_g = \{0, -g, 0, 0, 0, -g, 0, 0, \dots, 0, -g, 0, 0\}^T$$

In DyRoBeS the acceleration can be specified as acting in any direction in the global reference frame by specifying the x and y components of the gravity acceleration.

$$a_g = \{g_x, g_y, 0, 0, g_x, g_y, 0, 0, \dots, g_x, g_y, 0, 0\}^T \quad (12)$$

### **Preload :**

Preload is a constant point load applied at the AMB locations in a direction against the acceleration due to gravity. In active magnetic bearings, this force is due to the bias current in the magnetic bearings. This preload helps in aligning the rotor at the AMB locations such that, when the rotor is stationary, its center coincides with that of the AMB centerline. The preloads ' $F_{pn}$ ' (or bias currents for more general analysis) must be computed for the multi bearing support system. Figure 2 shows the influence of the gravity load and the preloads on the multi bearing rotor.

The other option is to account for the preload required by use of the bias current option in the DyRoBeS nonlinear force current AMB bearing model.

### **Forces After AMB Power Loss**

Rotating machinery supported by AMBs have a limited load capacity which is much less than a typical fluid-film bearing design. It is very difficult to predict the magnitudes of all the dynamic loads which the system will experience in service. Whenever the forces experienced by the rotor system exceed this AMB limit, the bearings may loose control of the rotor and fail in supporting it. Another reason for such a failure of the AMB system could be the loss of power supply to the bearings due to a variety of reasons. To design for such situations, AMB systems are provided with auxiliary or backup bearings which support the rotor in case of overload or untimely AMB power loss. These back-up bearings must withstand the high dynamic loads of the rotor and allow the system to operate until the problems can be rectified or for the system to bring the rotor to a standstill. Some of the forces in the rotor system change after AMB power

loss. The unbalance forces and gravity loads remain the same but the preloads at the AMB locations where the power is cut off will decay. The rotor drops onto the backup bearings due to the influence of unbalance and gravity. When the rotor contacts the back-up bearings, it may experience very high impact loads. The following sections describe each of these new forces in more detail.

### **Contact Force Between Shaft and Bearing:**

When the magnetic bearings in an AMB system are no longer active, the bearing forces which constrain the rotor decay rapidly. The other external forces like gravity and unbalance, acting on the system, make the rotor take a path away from the desired position within the bearing clearance space. For this reason, AMB systems are provided with auxiliary or back-up bearings which prevent damage to the machinery by keeping the rotor from hitting parts of the stator or magnetic bearings itself. The dynamic contact forces between the rotor and backup bearings are very high compared to the static reaction forces. These highly non-linear impact forces when the rotor is in contact with the bearings, can be calculated by modeling the contact dynamics using the Hertzian contact theory and the Coulomb's friction coefficient for sliding contact between the rotor and stator. This approach requires the knowledge of contact stiffness and damping at the rotor-stator interface.

### **Inner Race Rotation For The Case Of Anti-friction Bearings**

Anti-friction bearings are generally seen in machinery where load carrying capacity of the support systems must be high. They can sustain shock loads better than most other systems. These advantages have led many AMB system designers to use this style bearing as the back-up bearings. One of the aspects that have to be taken into consideration while modeling anti-friction bearings is the rotation of the bearing inner race due to the tangential contact forces acting at the contact point between the rotor and back-up bearing as shown in Fig. 3. The current version of DyRoBeS does not yet allow for inner race rotation. This effect will be accounted for in the following results by the use of a reduced friction coefficient at the point of contact. Initial test cases have produced a similar impact response, but additional work is required to properly account for the inner race contact dynamics (see reference 10 - 14).

### **Auxiliary Bearing with Multiple Layers of Contact Stiffness**

A general backup bearing and support system could be represented as shown in Fig 4. The contact stiffness can be treated as varying stiffness and damping parameters, as a function of deformation of the auxiliary bearing and the associated housing stiffness and damping.

The evaluation of the auxiliary bearing can be treated in DyRoBeS by a multiple segment description of the auxiliary bearing stiffness and damping. The initial non-contact stiffness gap is followed by one or more additional rings of stiffness and damping. The equations used for this purpose are presented in the following discussion.

### **Generalized Non-Linear Isotropic Bearings**

Two types of the generalized non-linear isotropic bearing are provided in this bearing option for DyRoBeS (2004). Given a (x,y) shaft displacement with  $r = \sqrt{x^2 + y^2}$ . The tangential velocity of the shaft, having a radius of R at the contact point, is given by

$$v_t = R\Omega + (-\dot{x}\sin\theta + \dot{y}\cos\theta) = R\Omega + \left(\frac{-\dot{x}y + \dot{y}x}{r}\right) \quad (13)$$

Consider that  $(-F_r)$  is the radial restoring force acting on the shaft due to displacement and  $(-F_t)$  is the tangential force due to Coulomb Friction:

$$-F_t = \mu(-F_r)\text{sign}(v_t) \quad (14)$$

The total forces action on the shaft due to displacement ( $r$ ), friction ( $\mu$ ), and linear damping ( $C$ ) are:

$$F_x = (-F_r)\cos\theta - (-F_t)\sin\theta - C\dot{x} \quad (15)$$

$$F_y = (-F_r)\sin\theta + (-F_t)\cos\theta - C\dot{y} \quad (16)$$

Two types of equations are provided in DyRoBeS ver 9.1 for the radial force and they are:

Case 1: Continuous Force-Displacement Curve

When  $r < r_0$  (deadband or gap)

$$F_r = 0, F_t = 0, F_x = 0, F_y = 0 \quad \text{No forces are acting on the shaft}$$

When  $r_0 \leq r$

$$F_r = k_0(r - r_0)^{a_0} + k_1(r - r_0)^{a_1} + k_2(r - r_0)^{a_2} + k_3(r - r_0)^{a_3} + k_4(r - r_0)^{a_4} \quad (17)$$

$$F_t = \mu F_r \text{sign}(v_t) \quad (18)$$

Note that  $r_0$  can be zero if no gap or deadband exists.

Case 2) Piecewise linear curves

When  $r < r_0$  (deadband or gap)

$$F_r = 0, F_t = 0, F_x = 0, F_y = 0 \quad \text{and no forces are acting on the shaft.}$$

When  $r_0 \leq r \leq r_1$

$$F_r = k_0(r - r_0) \quad (19)$$

$$F_t = \mu_0 F_r \quad (20)$$

When  $r_1 \leq r \leq r_2$

$$F_r = k_0(r_1 - r_0) + k_1(r - r_1) \quad (21)$$

$$F_t = \mu_1 F_r \quad (22)$$

When  $r_2 \leq r < r_3$

$$f_r = k_0(r_1 - r_0) + k_1(r_2 - r_0) + k_2(r - r_2) \quad (23)$$

$$F_t = \mu_2 F_r \quad (24)$$

When  $r_3 \leq r < r_4$

$$F_r = K_0(r_1 - r_0) + k_1(r_2 - r_1) + k_2(r_3 - r_2) + k_3(r - r_3) \quad (25)$$

$$F_t = \mu_3 F_r \quad (26)$$

When  $r_4 \leq r$

$$F_r = k_0(r_1 - r_0) + k_1(r_2 - r_1) + k_2(r_3 - r_2) + k_3(r_4 + r_3) + k_4(r - r_4) \quad (27)$$

$$F_t = \mu_4 F_r \quad (28)$$

This option gives the user the ability to specify the auxiliary bearing gap, contact stiffness which is the soft mounting stiffness and the limit stiffness after a given deformation. This is the option that has been utilized for the results presented in this paper.

## SPECIAL CONCERNS FOR MULTIPLE BEARING MACHINERY ANALYSIS

A continuous rotor system with multiple bearings is statically in-determinant and must be solved with the foundation support system stiffness characteristics. The AMB controller bias force produces a very stiff bearing static stiffness to center the rotor to the desired location within the clearance space. The loading will change as a function of the support stiffness. The more flexible the coupling(s) of multi-body systems, the less important will be this effect for two bearing components.

The actual bias loading on the non-drop AMB's during the initial rotor drop is also not easily determined. The non drop location bias loads are therefore not considered to change during the drop and resulting transient motion. The transient short duration impact forces that are generated are reacted by the dynamic stiffness and damping of any of the other active bearings still under control. Multiple bearing machines will likely have one controller for each set of two active bearings. A typical configuration could be a four bearing machine having a driver and compressor or pump for example. A double extended motor could be used to drive compressors or pumps on either end resulting in a six bearing support system and six or more backup bearings. It is possible to have four auxiliary bearings on a standard two bearing compressor or pump to better protect the stator if the shafting is very flexible. The rotor dynamics of multiple bearing, multiple body rotor systems with rigid or near rigid couplings is not documented in great detail for high speed machinery. Turbo-generator units with fluid-film bearings are the most likely machinery to have been solid coupled and documented with regard to loading and unloading of bearings due to alignment problems. The analysis of solid coupled multi-bearing machines is complicated by the number of modes that must be considered. For example the typical third mode or first free-free forward mode of a two-bearing machine becomes the seventh or higher forward mode for a six bearing rotor system that has essentially three bodies connected by two rigid couplings( see Example 4 in the following discussion of this paper).

The DyRoBeS computer program can evaluate a system with from one to 100 AMB supported bearings and 100 auxiliary bearings. Any number of AMB drop locations, from one to **100**, can be evaluated. The rotor model may contain up to 500 rotor stations. The computation time for a typical constant speed drop is 3 minutes or less using a 1.7 GHz Pentium IV processor. The evaluation of a changing speed or time dependent non-linear forcing will increase the execution time to several hours. The integration process can use either a Runge Kutta, a Newmark- $\beta$

method or a Wilson- $\theta$  calculation which can include numerical damping for higher modes (see Craig(1981, Bathe(1995)). The following discussion gives a brief review of the later two numerical methods.

### The Newmark- $\beta$ Method

The Newmark constant average acceleration method assumes the average acceleration in the time interval  $t_i$  to  $t_{i+1}=t_i+\Delta t$  to be the average value of the discrete initial and final accelerations.

$$\ddot{q}(t) = \frac{1}{2}(\ddot{q}_i + \ddot{q}_{i+1}) \quad (29)$$

Successive integration of equation (1) gives the velocity and displacement at time  $t_{i+1}=t_i+\Delta t$ .

$$\dot{q}_{i+1} = \dot{q}_i + \left(\frac{\Delta t}{2}\right)(\ddot{q}_i + \ddot{q}_{i+1}) \quad (30)$$

$$q_{i+1} = q_i + (\Delta t)\dot{q}_i + \left(\frac{\Delta t^2}{4}\right)(\ddot{q}_i + \ddot{q}_{i+1}) \quad (31)$$

Rearranging equations (30) and (31), the velocity and acceleration at time  $t_{i+1}=t_i+\Delta t$  are expressed as functions of displacement, velocity, acceleration at time  $t_i$  and displacement at time  $t_{i+1}=t_i+\Delta t$ .

$$\dot{q}_{i+1} = \left(\frac{2}{\Delta t}\right)(q_{i+1} - q_i) - \dot{q}_i \quad (32)$$

$$\ddot{q}_{i+1} = \left(\frac{4}{\Delta t^2}\right)(q_{i+1} - q_i) - \left(\frac{4}{\Delta t}\right)\dot{q}_i - \ddot{q}_i \quad (33)$$

The equations of motion are numerically integrated for each time step beginning with the initial conditions of  $q(0) = q_0$ ,  $\dot{q}(0) = \dot{q}_0$ . The initial accelerations are obtained from the dynamic equilibrium equation:

$$\ddot{q}_i = M^{-1}(\mathcal{Q}_i - \bar{C}\dot{q}_i - \bar{K}q_i) \quad (34)$$

The dynamic equilibrium is satisfied at both  $t_i$  and  $t_{i+1}$ . The equilibrium equations at time  $t_{i+1}$  may be written as follows:

$$M\ddot{q}_{i+1} + \bar{C}\dot{q}_{i+1} + \bar{K}q_{i+1} = \mathcal{Q}_{i+1} \quad (35)$$

Substitution of equations (32) and (33) into equation (35) gives a set of equations with displacements at time  $t_{i+1}$  to be determined.

$$\left(\bar{K} + \frac{2}{\Delta t}\bar{C} + \frac{4}{\Delta t^2}M\right)q_{i+1} = \hat{\mathcal{Q}}_{i+1} \quad (36)$$

and

$$\hat{\mathbf{Q}}_{i+1} = \mathbf{Q}_{i+1} + \mathbf{M} \left( \frac{4}{\Delta t^2} \mathbf{q}_i + \frac{4}{\Delta t} \dot{\mathbf{q}}_i + \ddot{\mathbf{q}}_i \right) + \bar{\mathbf{C}} \left( \frac{2}{\Delta t} \mathbf{q}_i + \dot{\mathbf{q}}_i \right) \quad (37)$$

Once the displacement at time  $t_{i+1}$  are solved from above equation (36), the velocity and acceleration at time  $t_{i+1}$  can be determined from equations (32) and (33).

### The Wilson- $\theta$ Method

The Wilson- $\theta$  method is essentially an extension of the linear acceleration method. The acceleration is assumed to be linear from time  $t_i$  to time  $t_i + \theta \Delta t$ , where  $\theta \geq 1.0$ . For unconditional stability in the linear problems,  $\theta$  must be greater than or equal to 1.37 and the value of 1.4 is usually employed. It has been shown that the optimal value of  $\theta$  is 1.420815. The acceleration from linear assumption is given as:

$$\ddot{\mathbf{q}}(t_i + \tau) = \ddot{\mathbf{q}}(t_i) + \frac{\tau}{\theta \Delta t} (\ddot{\mathbf{q}}(t_i + \theta \Delta t) - \ddot{\mathbf{q}}(t_i)) \quad (38)$$

Following the same procedures as described in Newmark- $\beta$  Method, the equilibrium equations at time  $t_i + \theta \Delta t$  may be written as follows:

$$\mathbf{M} \ddot{\mathbf{q}}(t_i + \theta \Delta t) + \bar{\mathbf{C}} \dot{\mathbf{q}}(t_i + \theta \Delta t) + \bar{\mathbf{K}} \mathbf{q}(t_i + \theta \Delta t) = \mathbf{Q}(t_i + \theta \Delta t) \quad (39)$$

Since the accelerations are assumed to be linear, a linearly projected load vector  $\mathbf{Q}(t_i + \theta \Delta t)$  is given by:

$$\mathbf{Q}(t_i + \theta \Delta t) = \mathbf{Q}(t_i) + \theta [\mathbf{Q}(t_i + \Delta t) - \mathbf{Q}(t_i)] \quad (40)$$

The displacements at time  $t_i + \theta \Delta t$  are solved from equation (39) after substitution and rearrangement:

$$\left( \bar{\mathbf{K}} + \frac{3}{\theta \Delta t} \bar{\mathbf{C}} + \frac{6}{(\theta \Delta t)^2} \mathbf{M} \right) \mathbf{q}(t_i + \theta \Delta t) = \hat{\mathbf{Q}}(t_i + \theta \Delta t) \quad (41)$$

and

$$\begin{aligned} \hat{\mathbf{Q}}(t_i + \theta \Delta t) = & \mathbf{Q}(t_i) + \theta [\mathbf{Q}(t_i + \Delta t) - \mathbf{Q}(t_i)] \\ & + \mathbf{M} \left( \frac{6}{(\theta \Delta t)^2} \mathbf{q}_i + \frac{6}{\theta \Delta t} \dot{\mathbf{q}}_i + 2\ddot{\mathbf{q}}_i \right) + \bar{\mathbf{C}} \left( \frac{3}{\theta \Delta t} \mathbf{q}_i + 2\dot{\mathbf{q}}_i + \frac{\theta \Delta t}{2} \ddot{\mathbf{q}}_i \right) \end{aligned} \quad (42)$$

It should be noted that both methods are unconditionally stable in the linear problems. That is, the solution is stable for any value of  $\Delta t$  in linear problems; however, the result may not be accurate. For the nonlinear problems, an iterative procedure such as Newton-Raphson iteration (Bathe, 1995) is required to ensure the dynamic equilibrium condition, equations (36) and (41), is satisfied. It is expected that smaller time steps produce better results. Larger time steps can decrease the accuracy of the solution and also can introduce some unwanted numerical oscillations in the solution. One must exhibit some care when using very small time steps so that the computational times are not excessive. However, for the highly non-linear case, a small time interval is necessary for the solution convergence. The time step suggested by many researchers

in the linear problems is about  $T_{cr}/20$  or smaller for stability reasons.  $T_{cr}$  is the natural period for the critical frequency. These direct integration methods have been discussed in Bathe (1995) and Craig (1981). Due to the similarity of the Newmark- $\beta$  and the Wilson- $\theta$  method, they can be implemented in a single computer subroutine or function.

## SPECIAL CONSIDERATION FOR STARTUP AND SHUTDOWN SIMULATION

There are two types of transient analysis. One is the rotor system with a constant rotational speed, and the other one is with a variable rotational speed. For a constant rotational speed, the transient analysis is used to determine the steady state response for the non-linear systems or the linear/nonlinear systems subject to sudden excitations. In many applications, there are needs to study the rotor motion during startup, shutdown, going through critical speeds, or rotor drop when the magnetic bearings failure occurred. In these situations, the angular velocity (spin speed) is no longer a constant and is a function of time. The governing equations of motion for a constant rotational speed have been presented before, the governing equations of motion for a variable rotational speed system are:

$$\begin{aligned} \mathbf{M}\ddot{\mathbf{q}}(t) + [\mathbf{C} + \dot{\phi} \mathbf{G}] \dot{\mathbf{q}}(t) + [\mathbf{K} + \ddot{\phi} \mathbf{G}] \mathbf{q}(t) \\ = \dot{\phi}^2 \mathbf{Q}_1(\phi) + \ddot{\phi} \mathbf{Q}_2(\phi) + \mathbf{Q}_3(\dot{\mathbf{q}}, \mathbf{q}, \phi, \dot{\phi}, \ddot{\phi}, t) \end{aligned} \quad (43)$$

Two more terms introduced in the governing equations due to the speed variation are: circulatory matrix  $\ddot{\phi} \mathbf{G}$  and forcing function  $\ddot{\phi} \mathbf{Q}_2$ . At any time instant, the angular velocity  $\dot{\phi} = \Omega$ . All the linearized damping and stiffness terms are in the damping and stiffness matrices and all the other interconnection nonlinear forces are included in  $\mathbf{Q}_3$ .  $\mathbf{Q}_1$  and  $\mathbf{Q}_2$  are functions of  $(\phi, \dot{\phi})$  and  $(\phi, \ddot{\phi})$ , respectively. For mass unbalance,  $\mathbf{Q}_1$  and  $\mathbf{Q}_2$  at station “ $r$ ” can be obtained from the following expression:

$$\begin{Bmatrix} F_{u,x} \\ F_{u,y} \\ M_{u,x} \\ M_{u,y} \end{Bmatrix} = \dot{\phi}^2 \begin{Bmatrix} m \cos \phi \\ m \sin \phi \\ 0 \\ 0 \end{Bmatrix} + \ddot{\phi} \begin{Bmatrix} m \sin \phi \\ -m \cos \phi \\ 0 \\ 0 \end{Bmatrix} \quad (44)$$

For a system with a constant rotational speed ( $\dot{\phi} = \Omega, \ddot{\phi} = 0$ ) and for a system with a variable rotational speed ( $\dot{\phi} = \Omega, \ddot{\phi} \neq 0$ ), the transient response can be obtained by direct numerical integration algorithms in the physical coordinates. For simplicity of notion, the equations of motion, equation (43) can be rewritten as:

$$\mathbf{M}\ddot{\mathbf{q}}(t) + \bar{\mathbf{C}} \dot{\mathbf{q}}(t) + \bar{\mathbf{K}} \mathbf{q}(t) = \mathbf{Q} \quad (45)$$

## EXAMPLE ROTOR DROP RESULTS

The results presented in this paper have considered the initial position of the rotor to be at the center of the bearings at the drop time with the gravity load acting. All of the AMB locations are assumed to be inactive and the only bearings in the system are the auxiliary bearings with the clearance gap. The rotor imbalance is also applied at this instant in time. This is considered to be a worst case condition for evaluation of the transient drop dynamics. The computation of the drop transient using the non linear AMB capability of DyRoBeS for a motor compressor system is currently being evaluated but none of those results can be included in this discussion. The following results will discuss the NEDO test rotor drop transients for assumed conditions at the auxiliary bearings, then the results of a former test rotor from Virginia Tech with 3 major disk locations, then with 5 disk locations to lower the free-free mode frequency, and finally a six bearing compressor-motor-compressor train evaluation.

### Example 1: The NEDO ISO test rotor configuration

The NEDO test rotor as modeled has a length of 0.851 m, mass of 25.963 kg and can operate at speeds to 30,000 rpm and higher. The diameter of the shaft at the AMB is 0.063 m and at the auxiliary bearing it is 0.0396 m. The rotor is shown in Fig 5 with the two bearing locations showing at the auxiliary bearing locations. The undamped critical speed map is given in Fig 6 and the free-free mode is observed to be above 40,000 rpm with the lower two modes being clearly rigid rotor modes for bearing stiffness levels below  $10E8$  N/m. The free-free mode shape is shown in Fig 7 to be 43152 cpm or 719 Hz. The constrained static deflection is presented in Fig 8, with a max deflection of 2.57  $\mu\text{m}$ , again indicating a rigid rotor design. The midspan imbalance is 5E-5 kgm for the following drop case results.

The results of the rotor drop at 30000 rpm and decel to 10000 rpm is given in Fig 9, where the 3D orbits show a well behaved drop, with only a small side movement. This is confirmed by the time traces of the bearing force and response for the first bearing location, station 7, given in Figs 10 and 11. The orbit x-y motion at station 7 and 20, bearing 1 and 2 respectively, show an initial bounce then rapid decay to a small motion. A drop at below the free-free mode is considered as a good design for AMB support rotors.

With the rotor speed increased to 50000 rpm, a 0.04 second drop at constant speed is shown in Fig 14. This shows increased activity at the bearing locations. The orbit trace and force transmitted at bearing 1 and 2 are presented in Figs 15-16 and 17-18. It clear in these force plots that the rotor rebounds from the bearing after the initial contact, and the forces are slightly higher than for the 40000 rpm drop. For the constant speed, the FFT spectrum is possible and it clearly shows energy at running speed but also at the free-free mode frequency. The largest spikes are for frequencies below 5000 cpm.

The result of a drop at 50000 and decel to 40000 rpm, during a one second time period, is given in Figs 21 – 25. The 3D rotor response clearly shows large whirling and the orbit plots for bearing one shows the rotor motion taking the entire clearance gap of the auxiliary bearing. The bearing reaction and response versus time clearly indicate the danger of coming down through the free-free, even at the rate of 10000 rpm per second. The peak force is in excess of 5000 N, while the static load is only 128 N and numerous peaks of 2000 N are observed for bearing one. The vertical motion goes from -172  $\mu\text{m}$  to 121  $\mu\text{m}$ . The gap clearance is only 100  $\mu\text{m}$  and the soft spring retainer goes very stiff at 170  $\mu\text{m}$ . A slow unloaded decel through this speed range would not be tolerated by the retainer bearings most likely.

#### Example 2: A 3 disk solid rotor.

Limited testing of soft mount solid bushing were conducted at Virginia Tech in the mid 1990's using a rotor similar to that shown in Fig 26. The free-free mode for this rotor is at 37000 cpm (615 Hz), while the actual rotor test speed was only 8000 rpm (133 Hz). The critical speed is similar to the NEDO rotor, in that the desirable operation speed range is below the free-free mode. This rotor has a length of 62.84 in (1.6 m) and a mass of 310 lb (141 kg). The auxiliary bearing diameter is 3.527 in (89.6 $\mu$ m). The results shown in Figs 28 – 31 show a well behaved drop and rapid reduction to a small response and force level. The rotor has a single 1.0 oz-in imbalance at midspan for this drop.

This simulation gives added confidence that drops below the free-free mode of a two bearing rotor system has a low risk for system damage. The assumption of proper bearing operation for the duration is assumed in these results. If a higher friction is in effect or a larger rotor imbalance, the results would show higher force levels without doubt, but safe operation would be expected for normal operating conditions. The actual test results agree with these conclusions.

#### Example 3: A 5 disk solid rotor

The rotor used in Example 3 was initially going to run with added disks at the outboard locations, making it a 5 disk rotor. The configuration is shown in Fig 32 and the critical speed map is given in Fig 33. The free-free mode is clearly lower, down to about 7400 cpm (123 Hz) as shown in Fig 34. The rotor has a mass of 540 lb (245 kg). The rotor has a 1.0 oz-in imbalance at midspan and 0.5 oz-in at 180 degrees at each outboard disk location for this drop. A snap decel gave reasonable results, but the 1 second decel from 9000 to 6000 rpm (see Fig 35) allowed a great increase in levels at 0.7 seconds into the decel, the levels were excessive and the computation stopped (see Figs 36 – 38). The build up in amplitude shows forces at near 1000 lb (4448 N) and a rapidly increasing spiral of the rotor response at the bearing and much greater at the overhang locations.

#### Example 4: A 3 body 6 bearing industrial configuration

The compressor-motor-compressor configuration shown in Fig 39 was evaluated for rotor drop several years ago using the Virginia Tech FEA transient analysis and found to be marginally acceptable. The results of a recent limited evaluation using DyRoBeS is presented as the final example for this discussion. The critical speed map is given in Fig 40 but the first free-free mode is not likely the mode of concern, rather the 7<sup>th</sup> forward circular mode of this plot. The lower modes are partial rigid body modes and are somewhat damped by the multiple bearing locations. The initial results found that the compressors had increased activity while the heavier motor had less response. This solid coupled train of equipment has a total mass of 2893 lb (1312.kg) and a total length of 16.5 ft (5 m). The system is supported on six AMBs and has six auxiliary bearings. The rotor has a single 1.0 oz-in imbalance at the motor and 0.5 oz-in at 180 degrees at the midspan of each compressor. The drop transient response at 12000 rpm shown in Fig 41, is similar to the former study drop result, with much greater activity at the compressors. The 14<sup>th</sup> mode (7<sup>th</sup> forward mode in fact) is shown in Fig 42, where all 3 bodies are in a connected (constrained) free-free mode shape. The drop at a speed very close to this mode 14 frequency does not give greatly increased levels of amplitude (see Fig 43). A slow decel through this speed region may in fact give a more violent response, but the present results do not indicate this to be true in fact. The actual operating speed was much lower and this is hence only of academic interest at this point. More detailed evaluations of such systems will be made in future studies of multi-bearing machinery.

## SUMMARY

The results of this paper confirm the large amplitudes of response and force to the auxiliary bearings for a drop near a single rotor free-free natural frequency. The rotor drop and decel studies using DyRoBeS have predicted an even higher level of response for the moderate decel rates through these critical speeds. The results from the analysis are easily reduced in graphic form for presentation at design review discussions. The program is capable of greater detail of the rotor system and the AMB bearing than previous specialized computer programs.

## REFERENCES

- 1) Bathe, K. J. , 1995, "Finite Element Procedures", Prentice-Hall, Inc.
- 2) Chen, W. J., 1998, "A Note on Computational Rotor Dynamics," ASME Journal of Vibration and Acoustics, Vol. 120, pp. 228-233.
- 3) Chen, W. J. and H. M. Chen, 1999, "Rotor Transient Response with Fault Tolerant Magnetic Bearings," Proceedings of Asia-Pacific Vibration Conference, Nanyang Technological University, pp. 53-58.
- 4) Craig, R. R., 1981, "Structural Dynamics: an Introduction to Computer Methods" John Wiley & Sons, Inc., pp. 452-455.
- 5) DyRoBeS, version 9.1, Eigen Technologies Inc., 2004.
- 6) Forsythe, G. E., Malcolm, M. A., and, Moler, C.B., 1977, "Computer Methods for Mathematical Computations," Prentice-Hall, Inc. pp. 129-147.
- 7) Fumagalli, M., Feeny, B., and Schweitzer, G., 1992, "Dynamics of Rigid Rotors in Retainer Bearings", Proceedings of The Third International Symposium on Magnetic Bearings, Alexandria VA, July, pp. 157-168.
- 8) Fumagalli, M., Varadi, P., and Schweitzer, G., 1994, "Impact Dynamics of High Speed Rotors in Retainer Bearings and Measurement Concept", Proceedings of Fourth International Symposium on Magnetic Bearings, August 1994, Zurich, pp. 239-244.
- 9) Gelin, A., Pugnet, J.M., and Hagopian, J.D., 1990, "Dynamic Behavior of Flexible Rotors with Active Magnetic Bearings on Safety Auxiliary Bearings", Proceedings of 3rd International Conference on Rotordynamics, Lyon, France, pp. 503-508.
- 10) Hilber, H.M., Hughes, T.J.R., and Taylor, R.L., 1977, "Improved Numerical Dissipation for Time Integration Algorithms in Structural Dynamics," Earthquake Engineering and Structural Dynamics, 5, pp. 283-292.
- 11) Ishii, T., 1990, "Transient Response Technique Applied to Active Magnetic Bearing Machinery During Rotor Drop", Master of Science Thesis, Mechanical Engineering Department, Virginia Tech, Virginia
- 12) Ishii, T., and Kirk, R.G., 1991, "Transient Response Technique Applied to Active Magnetic Bearing Machinery During Rotor Drop", ASME Conference Proceedings, DE-Vol. 35, pp. 191-200.
- 13) Kirk, R. G. "Evaluation of AMB Turbomachinery Auxiliary Bearings," *ASME Trans, Journal of Vibration and Acoustics* Vol. 121 , 2, 1999, pp. 156-161 .
- 14) Kirk, R.G., and Ishii, T., 1993, "Transient Rotor Drop Analysis of Rotors following Magnetic Bearing Power Outage", Proceedings of MAG '93, pp. 53-61.
- 15) Kirk, R., Raju, K. and Ramesh, K., May 1996, "Evaluation of AMB Rotor Drop Stability", The Eighth Workshop on Rotordynamic Instability Problems in High Performance Turbomachinery, Turbomachinery Laboratory, Texas A & M University, Texas.
- 16) Press, W.H., Flannery, B.P., Teukolsky, S.A. and Vetterling, W.T., 1989, "Numerical Recipes: The Art of Scientific Computing," Cambridge University Press.

- 17) Raju, K.V.S., Ramesh, K., Swanson, E.E. and Kirk, R.G., 1995, "Simulation of AMB Turbomachinery for Transient Loading Conditions", Proceedings of MAG '95, Alexandria, VA, pp. 227-235.
- 18) Raju, K., May 1996, "Finite-Element Based Non-linear Transient Response Analysis of AMB Turbomachinery", Master of Science Thesis, Mechanical Engineering Department, Virginia Tech, Virginia.
- 19) Ramesh, K., and Kirk, R.G., 1992, "Subharmonic Resonance Stability Prediction for Turbomachinery with Active Magnetic Bearings", Proceedings of the Third International Symposium on Magnetic Bearings, Alexandria, VA, pp. 113-122, 1992.
- 20) Schmied, J., Pradetto, J.C., 1992, "Behavior of a One Ton Rotor Being Dropped into Auxiliary Bearings", Proceedings of The Third International Symposium on Magnetic Bearings, Alexandria VA, July, pp. 145-156.
- 21) Swanson, E., Raju, K. and Kirk, R., 1996, "Test Results and Numerical Simulation of AMB Rotor Drop", IMechE 1996, England, C500/074, pp. 119.

## ACKNOWLEDGMENTS

This work was sponsored by the Virginia Tech Rotor Dynamics Laboratory Industry Affiliates Group.

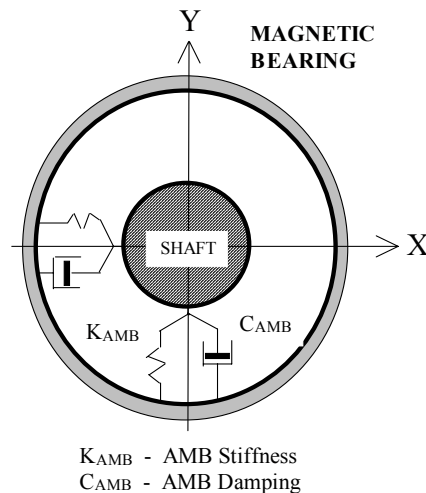


Fig. 1: Schematic Showing the AMB Assumed Linear Stiffness and Damping.



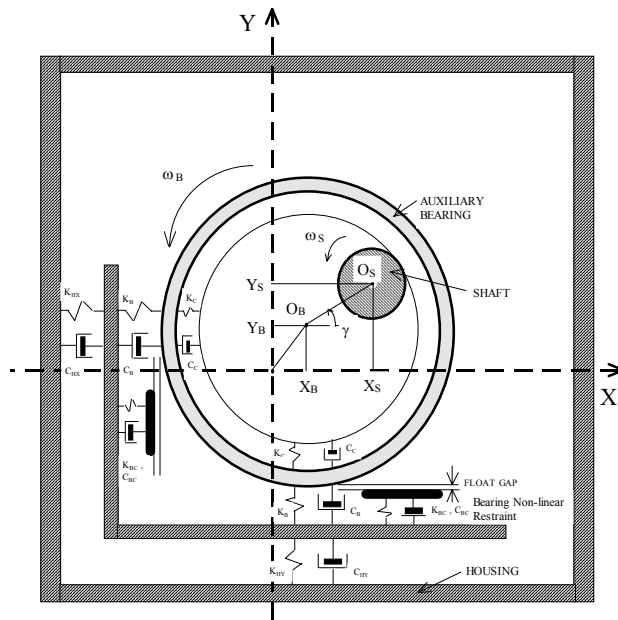


Fig. 4: Schematic of the cross-section of any typical AMB system at the back-up bearing.

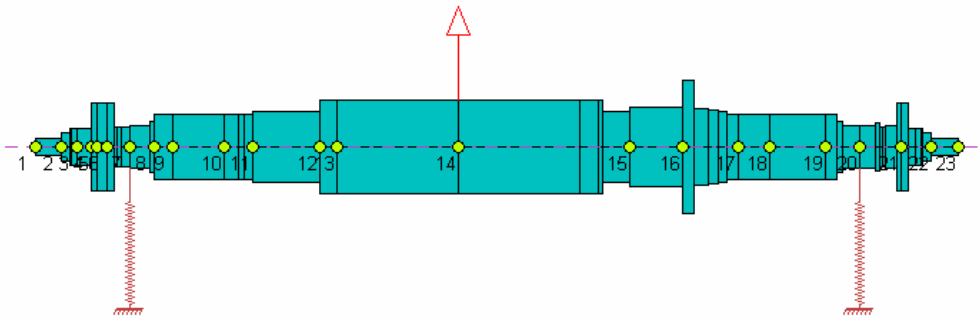


Fig 5 NEDO ISO Test Rotor

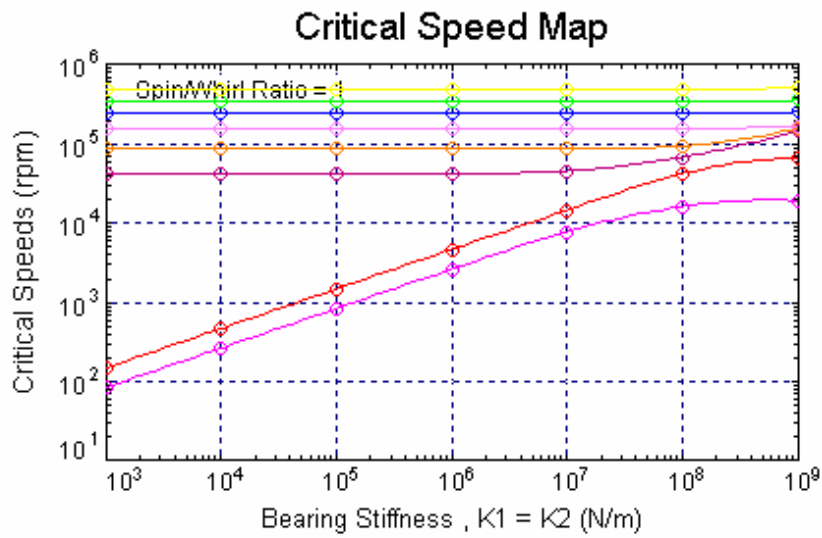


Fig 6 NEDO Test Rotor Undamped Critical Speed Map

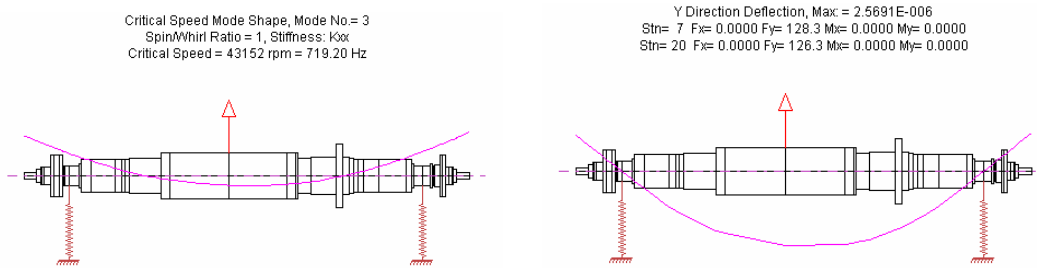


Fig 7 Test Rotor Free-Free Mode

Fig 8 Test Rotor Static Deflection

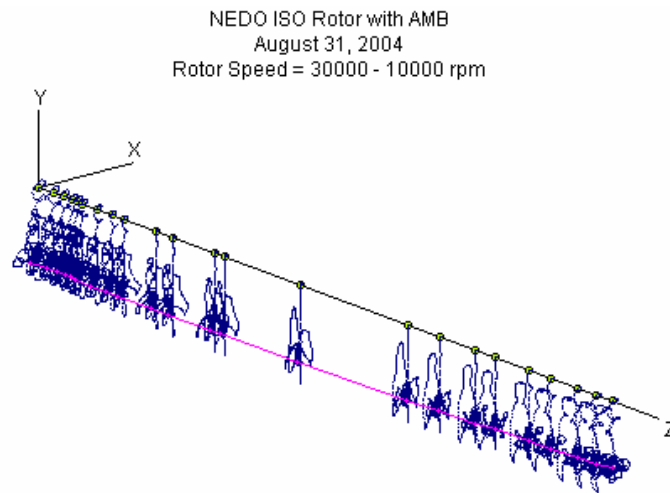


Fig 9 Test Rotor 3D Station Orbits for Drop at N = 30 000 and decel to 10 000 rpm

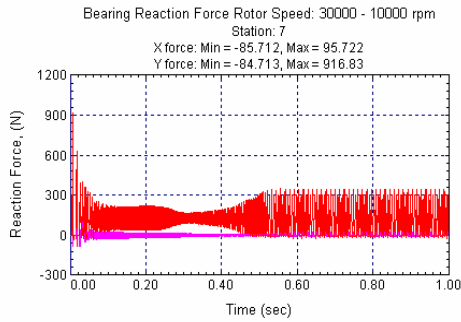


Fig 10 Sta 7 Brg 1 Force vs time, 30k to 10k rpm

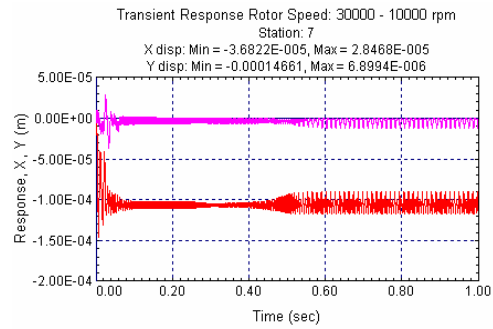


Fig 11 Sta 7 Brg 1 Force vs time, 30k to 10k rpm

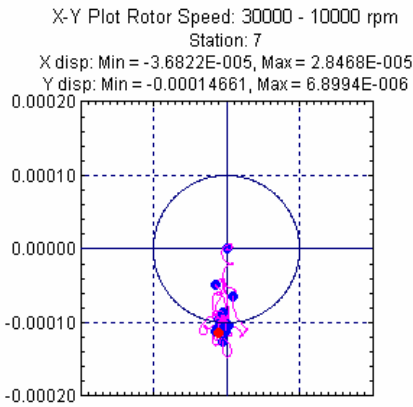


Fig 12 Brg 1 Orbit for Drop, 30k to 10k rpm

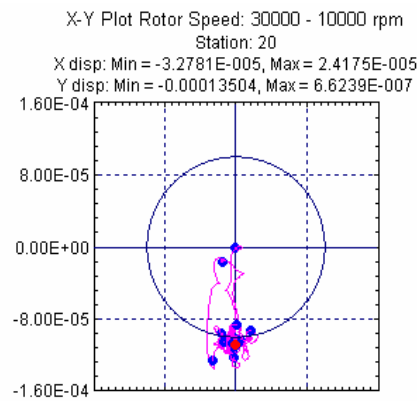


Fig 13 Brg 2 Orbit for Drop, 30k to 10k rpm

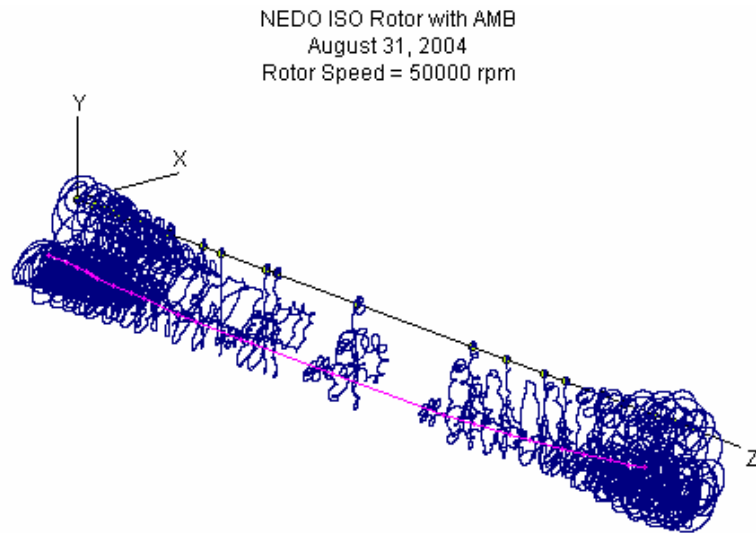


Fig 14 Test Rotor 3D Station Orbits for Drop at N = 50 000

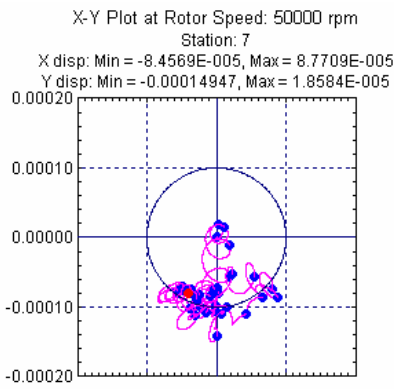


Fig 15 Brg 1 Orbit for Drop, 50k rpm

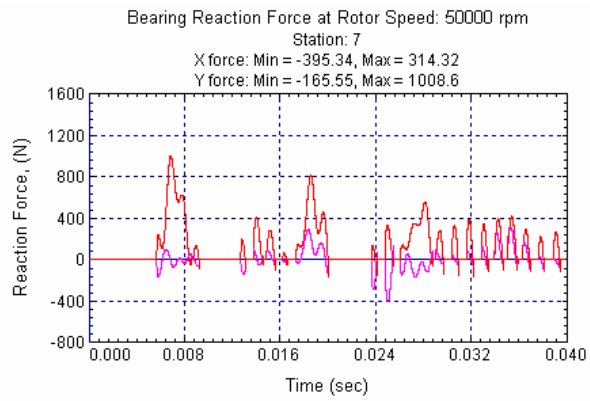


Fig 16 Brg 1 Force for Drop, 50k rpm

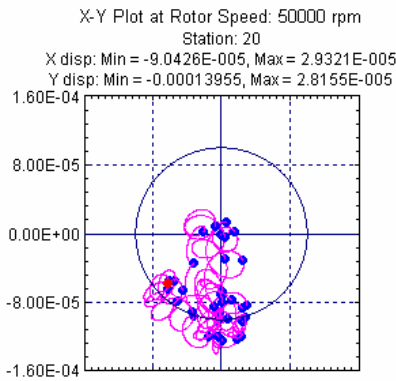


Fig 17 Brg 2 Orbit for Drop, 50k rpm

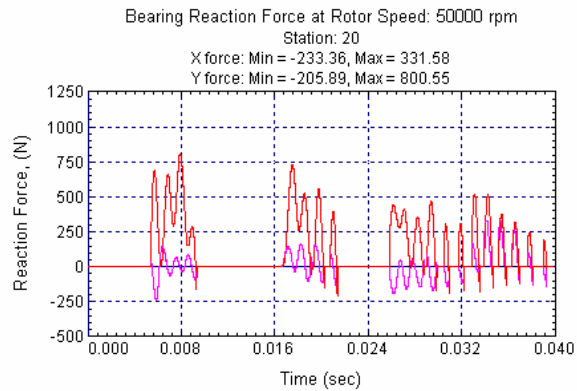


Fig 18 Brg 2 Force for Drop, 50k rpm

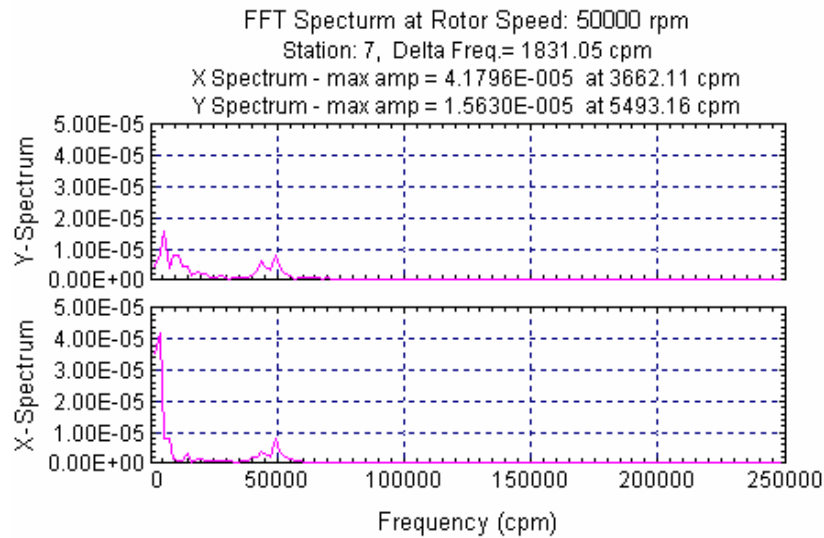


Fig 19 Brg 1 FFT for Drop, 50k rpm

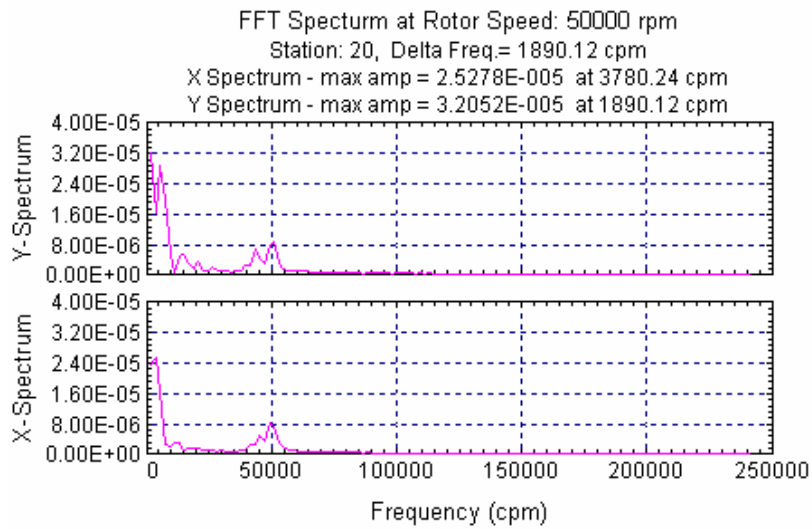


Fig 20 Brg 2 FFT for Drop, 50k rpm

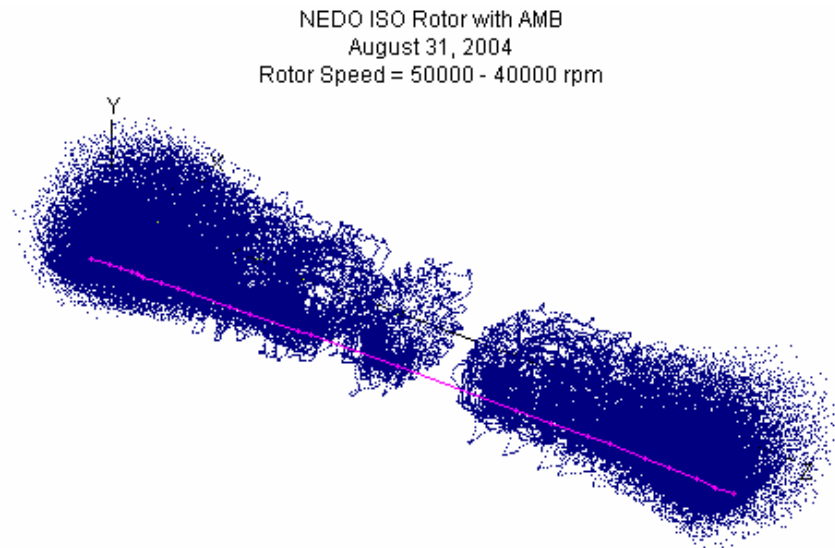


Fig 21 Test Rotor 3D Station Orbits for Drop at N = 50 000 and Decel to 40 000 rpm

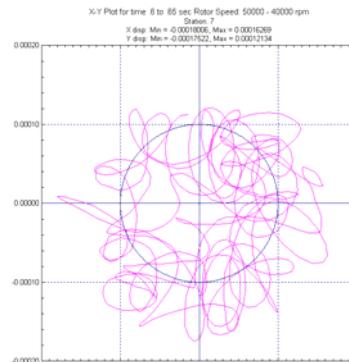
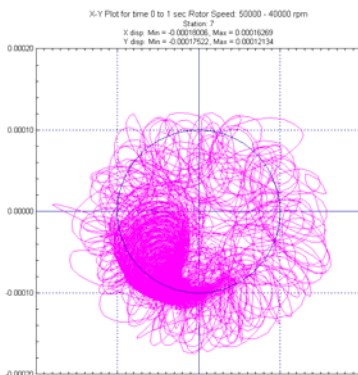


Fig 22 Brg 1 Orbit for Drop, Decel 50k-40k rpm

Fig 23 Brg 1 Partial Orbit for Drop, 50k-40k rpm

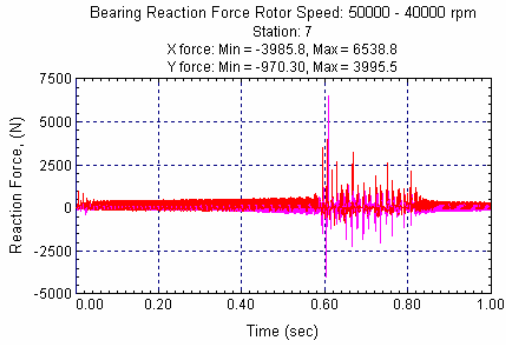


Fig 24 Brg 1 Reaction for Drop, 50k-40k rpm

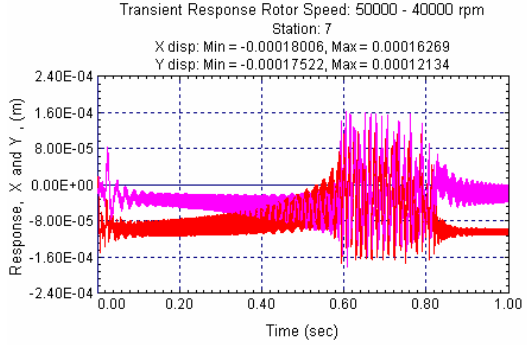


Fig 25 Brg 1 Response for Drop, 50k-40k rpm

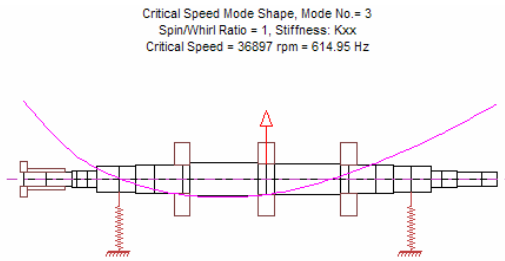


Fig 26 3 Disk VT Rotor, free-free mode shape

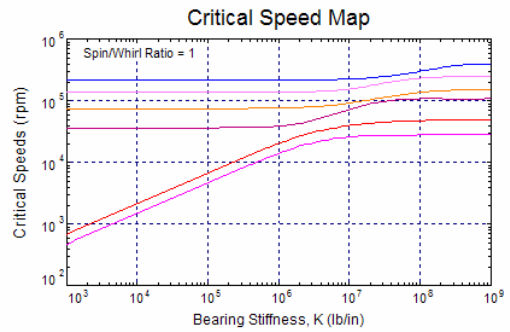


Fig 27 3 Disk VT Rotor, Critical Speed Map

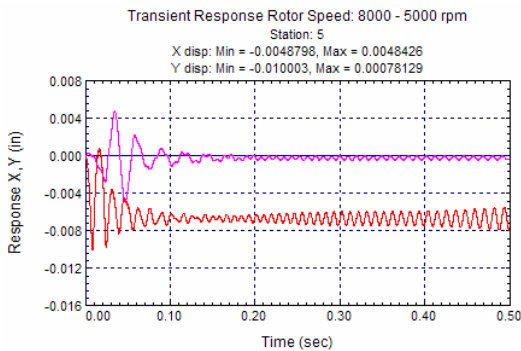


Fig 28 3 Disk VT, Brg 1 Response 8k -5k rpm

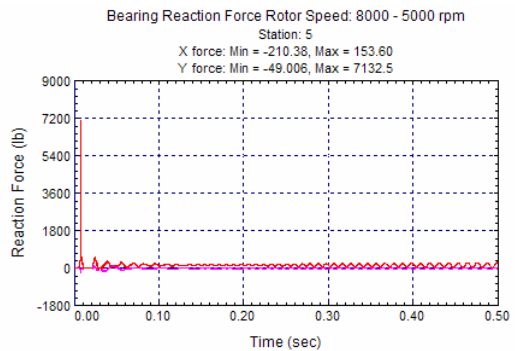


Fig 29 3 Disk VT, Brg 1 Force for 8k-5k rpm

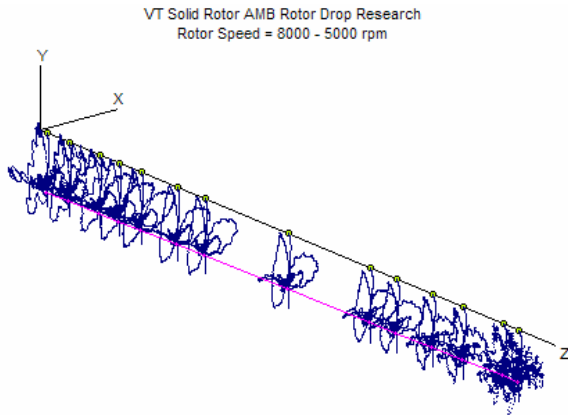


Fig 30 3 Disk VT, Drop 8k -5k rpm

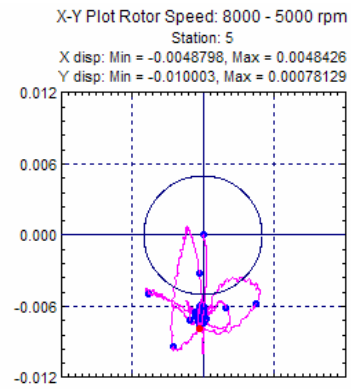


Fig 31 3 Disk VT, Brg 1 Orbit for 8k-5k rpm

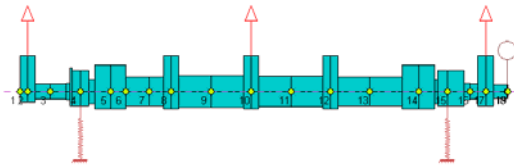


Fig 32 5 Disk VT Rotor model

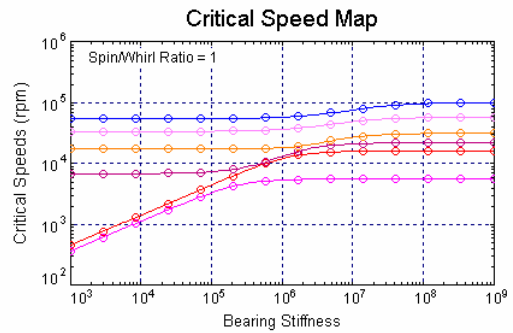


Fig 33 5 Disk VT Rotor, Critical Speed Map

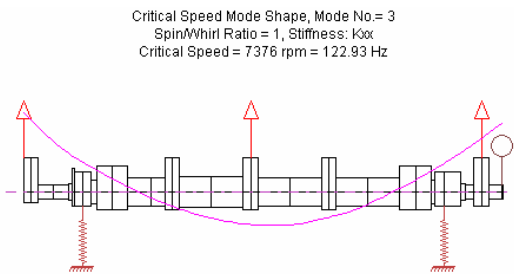


Fig 34 5 Disk VT Rotor, free-free mode shape

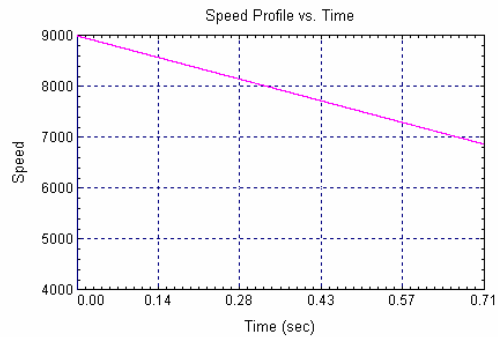


Fig 35 5 Disk VT Rotor, Speed versus time

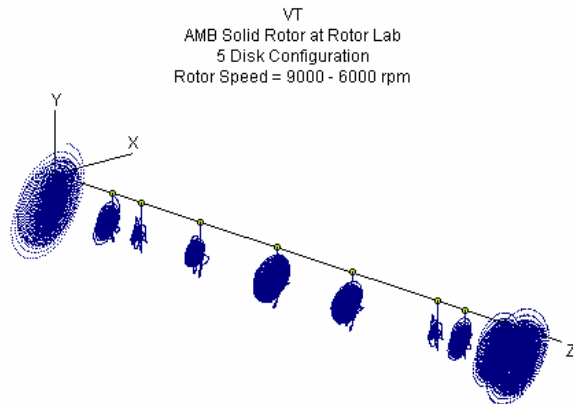


Fig 36 5 Disk VT Rotor Transient for decel from 9000 to 6800 rpm

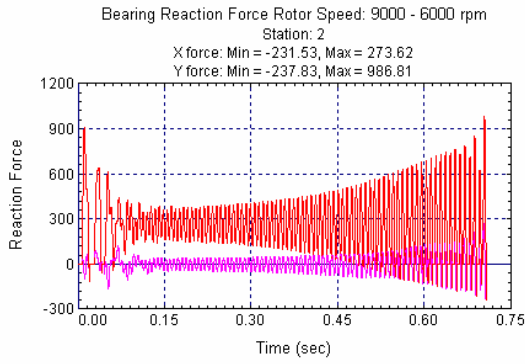


Fig 37 5 Disk VT Rotor, brg 1 Reaction Force

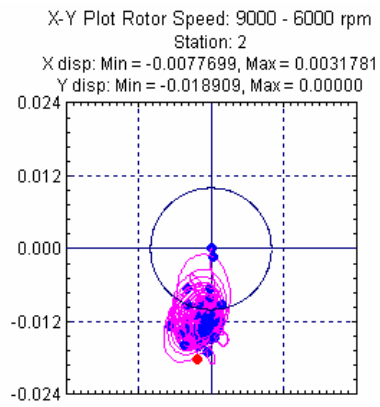


Fig 38 5 Disk VT Rotor, Brg 1 Orbit

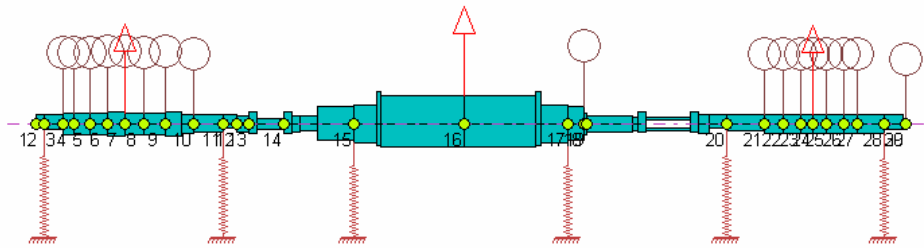


Fig 39 6 Brg 3 Rotor model for drop simulation

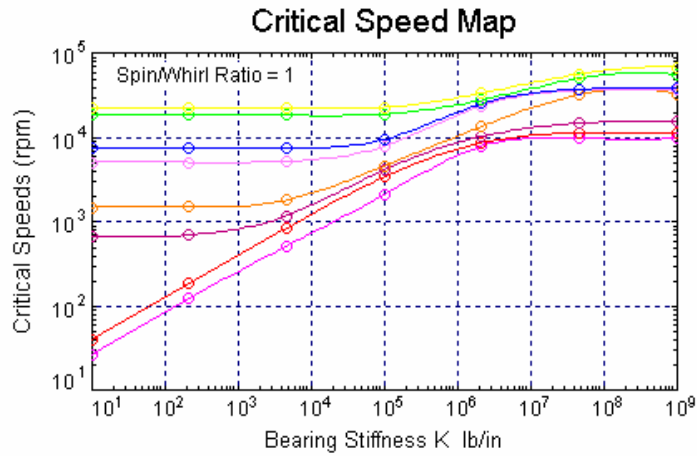


Fig 40 6 Brg 3 Rotor, Ncr Map

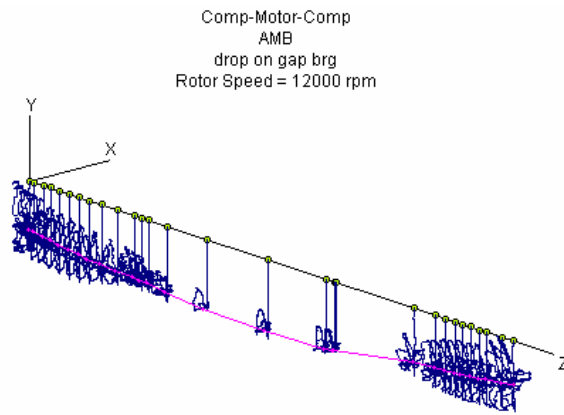


Fig 41 6 Brg 3 Rotor, Transient Response for a drop at 12000 rpm

Precessional Mode Shape - STABLE FORWARD Precession  
 Shaft Rotational Speed = 12000 rpm, Mode No.= 14  
 Whirl Speed (Damped Natural Freq.) = 19133 rpm, Log. Decrement = 0.1498

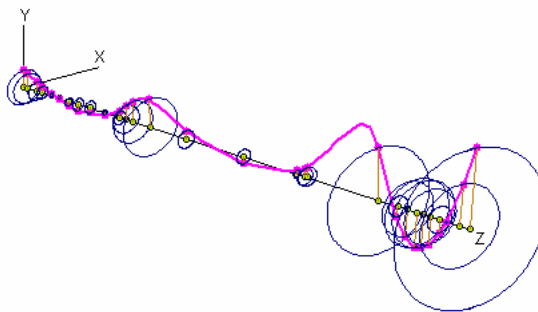


Fig 42 6 Brg 3 Rotor, 14<sup>th</sup> Damped Mode when N = 12000 rpm

Comp-Motor-Comp  
 AMB  
 drop on gap brg  
 Rotor Speed = 19143 rpm

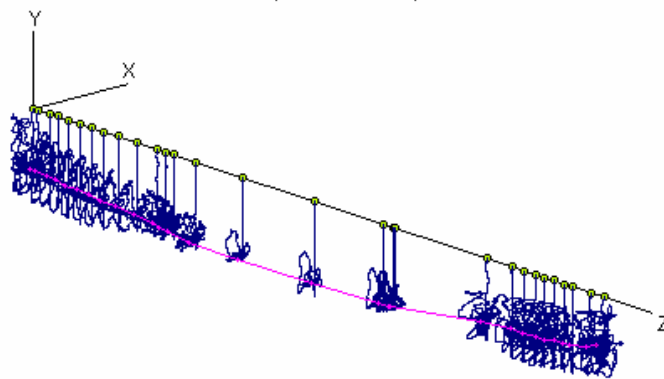


Fig 43 6 Brg 3 Rotor, Transient Response for a drop at 19143 rpm